Scientific Research Publishing

Optics and Photonics Journal, 2022, 12, 171-189
https://www.scirp.org/journal/opj
ISSN Online: 2160-889X
ISSN Print: 2160-8881

Controlling the Bandgaps of One-Dimensional TiO_2/SiO_2, TiO_2/SnO_2, and SiO_2/SnO_2 Photonic Crystals Using the Transfer Matrix Method

Fatimah Alamrani*, Edreese Alsharaeh

College of Science and General Studies, Alfaisal University, Riyadh, Saudi Arabia
Email: *falamrani@alfaisal.edu

How to cite this paper: Alamrani, F. and Alsharaeh, E. (2022) Controlling the Bandgaps of One-Dimensional TiO_2/SiO_2, TiO_2/SnO_2, and SiO_2/SnO_2 Photonic Crystals Using the Transfer Matrix Method. *Optics and Photonics Journal*, **12**, 171-189.
https://doi.org/10.4236/opj.2022.127013

Received: May 27, 2022
Accepted: July 26, 2022
Published: July 29, 2022

Abstract

One-dimensional photonic crystals (1D PhCs) have a unique ability to control the propagation of light waves, however certain classes of 1D oxides remain relatively unexplored for use as PhCs. Specifically, there has not been a comparative study of the three different 1D PhC structures to compare the influence of layer thickness, number, and refractive index on the ability of the PhCs to control light transmission. Herein, we use the transfer matrix method (TMM) to theoretically examine the transmission of 1D PhCs composed of layers of TiO_2/SiO_2, TiO_2/SnO_2, SiO_2/SnO_2, and combinations of the three with various top and bottom layer thicknesses to cover a substantial region of the electromagnetic spectrum (UV to NIR). With increasing layer numbers for TiO_2/SiO_2 and SiO_2/SnO_2, the edges became sharper and wider and the photonic bandgap width increased. Moreover, we demonstrated that PhCs with significantly thick TiO_2/SiO_2 layers had a high transmittance for a wide bandgap, allowing for wide-band optical filter applications. These different PhC architectures could enable a variety of applications, depending on the properties needed.

Keywords

One-Dimensional Photonic Crystal, Photonic Bandgap, Transfer Matrix Method, Optical Filter, Metal Oxides

1. Introduction

Photonic crystals (PhCs) are synthetic materials that can uniquely manipulate light propagation across different length scales [1], and are therefore useful for a wide range of applications such as optical filters, lasers, waveguides, solar energy

applications, optical switches, and light-emitting diodes (LEDs) [2] [3] [4] [5] [6]. Because of their low cost and ease of fabrication, lD PhCs composed of alternating layers of high and low dielectric constant material are the most researched and applied PhCs, and have been gaining in popularity as Bragg mirrors, thermal sensors, energy-saving spectrally-selective coatings, anti-glare side view car mirrors, transparent heat reflectors, thermal collectors, optical filters, and structural colors because of their intriguing optical properties [7]-[12]. For 1D PhCs, the position of the transmission spectra and the intensity of the reflectance peak are influenced by the thickness, number, and refractive index of the layers. The greater the dielectric constant difference between the structural layers, the fewer the layers required to achieve a given reflectance value, which allows for optical filtering applications to be targeted [13]. From a lattice dynamics standpoint, the Bragg scattering bandgap and local resonant bandgap principles are confirmed for 1D PhCs [14].

Optical filters allow us to extract required signals without the use of electrical circuits, and common optical filters include Fabry–Perot interferometers, waveguide Bragg gratings, and Mach–Zehnder interferometers [15]. However, these are not suitable for optical integrated circuits due to their large area. On the other hand, PhC filters perform significantly better than previous systems, with benefits such as ease of fabrication, quick modulation, low-cost material composition, and sharp and smooth optical transitions [16] [17]. For example, SP Singh *et al.* [18] used the transfer matrix method (TMM) to create 1D optical filters from GaP and GaSb. The effect of disorder on the transmission spectrum of electromagnetic waves has been investigated using the transfer matrix method in one-dimensional multi-layered structures containing ferroelectric materials, such as $LiTaO_3$ [19]. This and other studies have shown that there is a high level of agreement between TMM simulations and physical experiments [20]. This suggests that TMM simulations could be used to elucidate the promise of other materials as 1D PhC optical filters.

Theoretical investigations have recently enabled the development of novel types of PhC devices, such as all-optical switches, two-state and many-state memory, all-optical limiters, all-optical modulators, and all-optical transistors. Significant research has focused on designing innovative PhC architectures into each functional layer of the solar cell to boost device performance. These optical structures feature one-of-a-kind qualities that bring up new possibilities for a wide range of applications. However, there are holes in the literature regarding comparative studies of 1D PhCs structures in regards to the influence of layer thickness, number, and refractive index on the ability of the PhCs to control light transmission. Metal oxides such as TiO_2, SiO_2, and SnO_2 have emerged as critical materials for high-performance optoelectronics [21] [22] [23], and we, therefore, explored their optical filtering performance as 1D PhCs using TMM simulations. The main objective of this theoretical analysis was to define and compare the influence of layer thickness, number, and refractive index on the

ability of the PhCs to control light transmission for optical filtering and photovoltaic applications. We found stark differences between layered 1D PhCs composed of different combinations of the three metal oxides that helped identify materials trends potentially promising for crating optical filters with different controllable properties. This work paves the way for improved optical filters and confirms the value of TMM simulations for screening the properties of various theoretical 1D PhCs.

2. Methodology

We must develop methods for examining multilayers in order to understand their fundamental properties [24] [25], and plane-wave propagation in an isotropic homogeneous medium is the most basic case. An important approach for studying the interaction between incident electromagnetic waves and 1D PhC layers is TMM, as it is the most widely used method for mathematically studying wave transmission in 1D materials [26].

TMM can be used to measure the transmission and reflection of incident electromagnetic waves across a multilayer periodic system, such as 1D PhCs made up of two layers of two different dielectric materials that are repeated in N unit cells in a periodic pattern. We utilize different materials and 1D PhCs structures (**Figure 1**) and theoretically compute the transmission of light from 300 nm up to 2500 nm using TMM. Specifically, our structures are made up of layers that are repeated N times and are only periodic in the x-direction, hence they are 1D PhCs. We specify the thickness (d_1, d_2) and refractive index (n_1, n_2) of two PhC dielectric materials (chosen from TiO_2, SiO_2, and SnO_2) with different refractive indexes (A and B layers), and the medium is homogeneous in the z-direction such that Snell's law is followed at each interface (*i.e.*, $n_1 \sin\theta_1 = n_2 \sin\theta_2$).

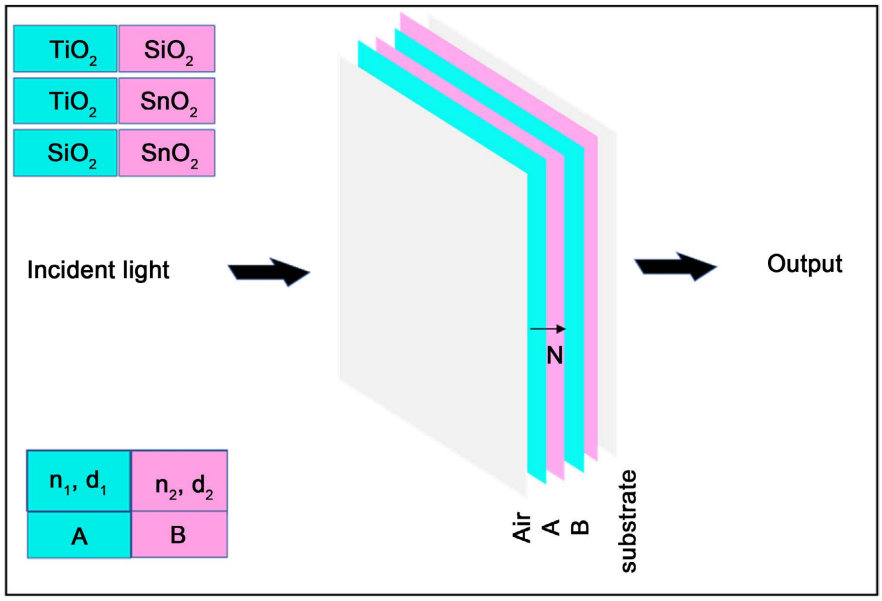

Figure 1. A schematic representation of our design of a 1D PhC repeated for N layers.

The following are the dynamical matrices for the transverse electric, *TE*, mode used in our TMM simulations:

$$D_m^{TE} = \begin{bmatrix} 1 & 1 \\ n_m & -n_m \cos\theta_m \end{bmatrix}, m = 1, 2 \tag{1}$$

where $m = 0, 1, 2$ denotes air, and the first and second layer, respectively, θ_m is the angle of the incidence for each layer, ω is the angular frequency, c is the electromagnetic (EM) wave speed in a vacuum, and n_m is the refractive index.

Each layer's propagation matrix is given as:

$$P_m = \begin{bmatrix} e^{-ik_m b_m} & 0 \\ 0 & e^{-ik_m b_m} \end{bmatrix}, m = 1, 2 \tag{2}$$

where $k_m = \omega n_m \cos\theta_m / c$ is the is the wave vector value.

Each periodic layer's transfer matrix is written as:

$$M_p = D_1 P_1 D_1^{-1} D_2 P_2 D_2^{-1} \tag{3}$$

After multiplying all of the individual transfer matrices for the overall periods (N) of the structures, we get:

$$M = \begin{pmatrix} M_{11} & M_{12} \\ M_{21} & M_{22} \end{pmatrix} = D_0^{-1} M_p^N D_0 \tag{4}$$

where D_0 is the air dynamical matrix.

The characteristic matrix $M[d]$ of one period is given by:

$$M[d] = \prod_{i=1}^{l} \begin{bmatrix} \cos\varphi_i & \dfrac{-i\sin\varphi_i}{p_i} \\ -ip_i \sin\varphi_i & \cos\varphi_i \end{bmatrix} = \begin{bmatrix} M_{11} & M_{12} \\ M_{21} & M_{22} \end{bmatrix} \tag{5}$$

where $\varphi = k|d|$, and l represents the layers of refractive index.

The characteristic matrix of the medium is given by:

$$\begin{aligned} M^N &= \begin{bmatrix} M_{11}U_{N-1}(q) - U_{N-2}(q) & M_{12}U_{N-1}(q) \\ M_{21}U_{N-1}(q) & M_{22}U_{N-1}(q) - U_{N-2}(q) \end{bmatrix} \\ &\equiv \begin{bmatrix} m_{11} & m_{12} \\ m_{21} & m_{22} \end{bmatrix} \end{aligned} \tag{6}$$

The Chebyshev polynomials of the second kind are:

$$UN(q) = \frac{\sin\left[(N+1)\cos^{-1} q\right]}{\left[1-q^2\right]^{1/2}} \tag{7}$$

where $q = 1/2\left[M_{11} + M_{22}\right]$.

The following equation gives the transmission value:

$$T = \left(\frac{1}{M_{11}}\right)^2 \tag{8}$$

In terms of the transmission coefficient, t, and the transmissivity of this structure can be stated as:

$$T = \frac{p_s}{p_0}|t|^2 \tag{9}$$

The transmission coefficient, t, of the multilayer is given by:

$$t = \frac{2p_0}{(m_{11} + m_{12}p_0)p_0 + (m_{21} + m_{22}p_0)} \tag{10}$$

where $p_0 = n_0\cos\theta_0 = \cos\theta_0$ is the propagation vector. The absorptance, A, is defined as the fraction of energy released and is calculated by $A = 1 - R - T$, where R is the reflectance. The formulas for r and t may be used to show that $R + T = 1$ for dielectric systems with real n_1 and n_2 according to energy conservation.

To simplify the calculations, we focus on the electromagnetic transmission of the PhC's. This study concentrates on transmission, as it is the most relevant for various optical applications including the design of optical filters. MATLAB was used and code was written to calculate various factors that affect the performance of the PhCs, such as the ambient medium (n_0), the refractive index of the substrate (n_s), the incidence angle (θ), the wavelength range (λ), the number of bilayers (N), and the film thickness (d).

3. Theoretical Results and Discussion

PhCs have refractive indexes that change in the same order as the wavelength of light, where the electromagnetic radiation cannot propagate for a specified range of energies and wave vectors [27]. PhCs rely on the phenomenon of slow group velocity photons, also known as "slow" light that occurs when the group velocity of light is reduced near the photonic bandgap, which can increase the degree of light absorption is useful for optical filtering [1] [28]. While PhCs can be prepared from different materials, the most common wide-bandgap oxides used in electronics and optical devices are TiO_2, SiO_2, and SnO_2 because of their high sensitivity to a wide range of optical wavelengths, simple manufacturing methods, low cost, and excellent compatibility with other parts and processes. We therefore explore the theoretical modeling of PhCs composed of alternating layers of these metal oxides thin films. All materials used herein are non-magnetic, homogeneous, and isotropic, and the different parameters included in this study are summarized in **Table 1**.

1) 1D TiO_2/SiO_2 PhCs

Photonic multilayer films such as TiO_2/SiO_2 are commonly manufactured for third-generation photovoltaic cells by alternately evaporating these high and low refractive index materials under high vacuum conditions [29] [30] [31] [32] [33]. TiO_2/SiO_2 has a high refractive index contrast, good passivity, and the ability to provide a conductive pathway, and has therefore been widely used experimentally [34]. Moreover, various SiO_2/TiO_2 stacks have been simulated using TMM for near-ultraviolet reflective and near-infrared anti-reflective filters [35]. Generally, these earlier studies only covered wavelengths up to 1500 nm, which suggested there was a need to examine a longer range of wavelengths. We therefore

Table 1. The materials and parameters studied via TMM simulation.

Wavelength (300 - 2500 nm), Angles (0˚), $n_0 = n_s = Air = 1$			Composite structures	
Photonic crystals	**Refractive index**		**Constant**	**Variables**
Structure 1	TiO_2/SiO_2	$n_1 = 2.6142/$ $n_2 = 1.4585$	1) Thickness 50/50 nm	$N = 1, 2, 4, 6, 8$
Structure 2	TiO_2/SnO_2	$n_1 = 2.6142/$ $n_2 = 2.0$	2) Top layer constant d_1, $N = 8$	50/50 nm 50/100 nm 50/150 nm
Structure 3	SiO_2/SnO_2	$n_1 = 1.458/$ $n_2 = 2.0$	3) Bottom layer constant d_2, $N = 8$	100/150 nm 150/150 nm 300/150 nm 500/150 nm 800/150nm

use TMM to simulate the optical properties of the TiO_2/SiO_2 layers from 300 - 2500 nm (Figure 1). TMM is regarded as one of the most suitable methods for investigating the interaction between incident electromagnetic waves and 1D PhC structures composed of different layers (N). In most studies, we can see only one photonic bandgap in the visible region, but by controlling the number of layers and the thickness, we were able to observe different bands in our study.

We investigated the effect of increasing the number of TiO_2/SiO_2 layers from 1 to 8 and the corresponding transmission curves. We chose a simple structure a TiO_2/SiO_2 thickness of 100 nm (50 nm/50 nm) for each layer in order to investigate the effect of multiple layers on the position and width of photonic bandgaps. There were visible differences in transmission spectra as the number of layers increased from 1 to 8 (Figure 2). At 8 layers, we observed the lowest transmission curve through the photonic bandgap area, while the rest of the curve still had a high transmission value. While 1 and 2 layers did not show photonic bandgaps, there was no clear interference through the rest of the transmission curves. The position of the photonic bandgaps in these two cases begins at longer wavelengths and then shifts to shorter wavelengths as the number of layers increases. We can also see that the width of the photonic bandgap was wider at higher layer numbers (*i.e.*, $N = 8$). After 8 layers, there was no discernible differences in bandgap width, and therefore we utilized $N = 8$ in the following sections.

2) 1D TiO_2/SnO_2 PhCs

Metal oxides such as SnO_2 have promise as primary materials in advanced applications in the optical, electronic, optoelectronic, and biological domains [36]. SnO_2 has a bulk bandgap of 3.6 eV (at room temperature), and has long been used as an opacifier and white colorant in ceramic glazes. Moreover, according to Diego Lopez-Torres *et al.* [37], SnO_2 is highly sensitive to humidity variations

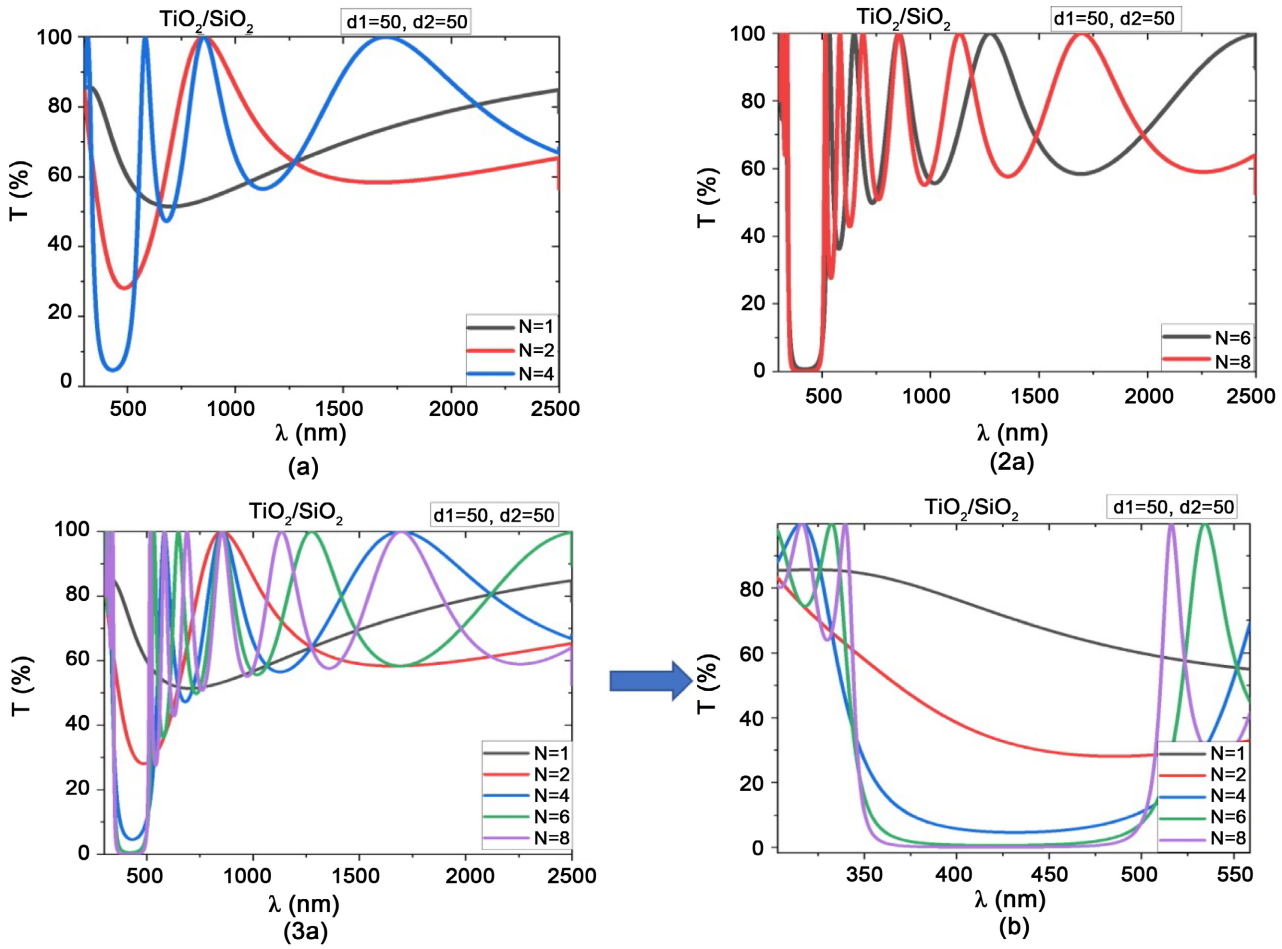

Figure 2. (a) The whole transmission spectrum for TiO_2/SiO_2 1D PhCs with varying numbers of layers ($N = 1$ to 8). (b) The bandgap region of (a) can be magnified to explain the widths and positions of each curve at varying layer numbers.

and can be used to increase the sensitivity of sensors based on PhC fibers. For example, SnO_2 does not require heating to function on an optical fiber, while the majority of metallic oxides require temperatures greater than 150˚C to function [38].

We used TMM to explore the changes in transmission curves when increasing the number of TiO_2/SnO_2 layers from 1 to 8. Like for TiO_2/SiO_2, we used a thickness of 100 nm (50 nm/50 nm) for each layer in order to investigate the effect of multiple layers on the position and width of photonic bandgaps (**Figure 3**). Increasing the number of layers from 1 to 8 caused the bandgap to widen. At $N = 8$, the transmission curve through the area of the photonic bandgap is the lowest, while the transmission of the curve was still high. At $N = 1$ and 2, the transmission curve began to appear at 450 nm with a modest peak. However, between $N = 6$ and 8, this peak flips into a broad photonic bandgap. Overall, the peaks are shifted to lower wavelengths at higher layer numbers. Interestingly, the band-edge is not as sharp as it is in the SiO_2 system, as the transition is smooth. Moreover, $N = 8$ has the lowest T value, which is close to zero and may reflect nearly 100% of the light.

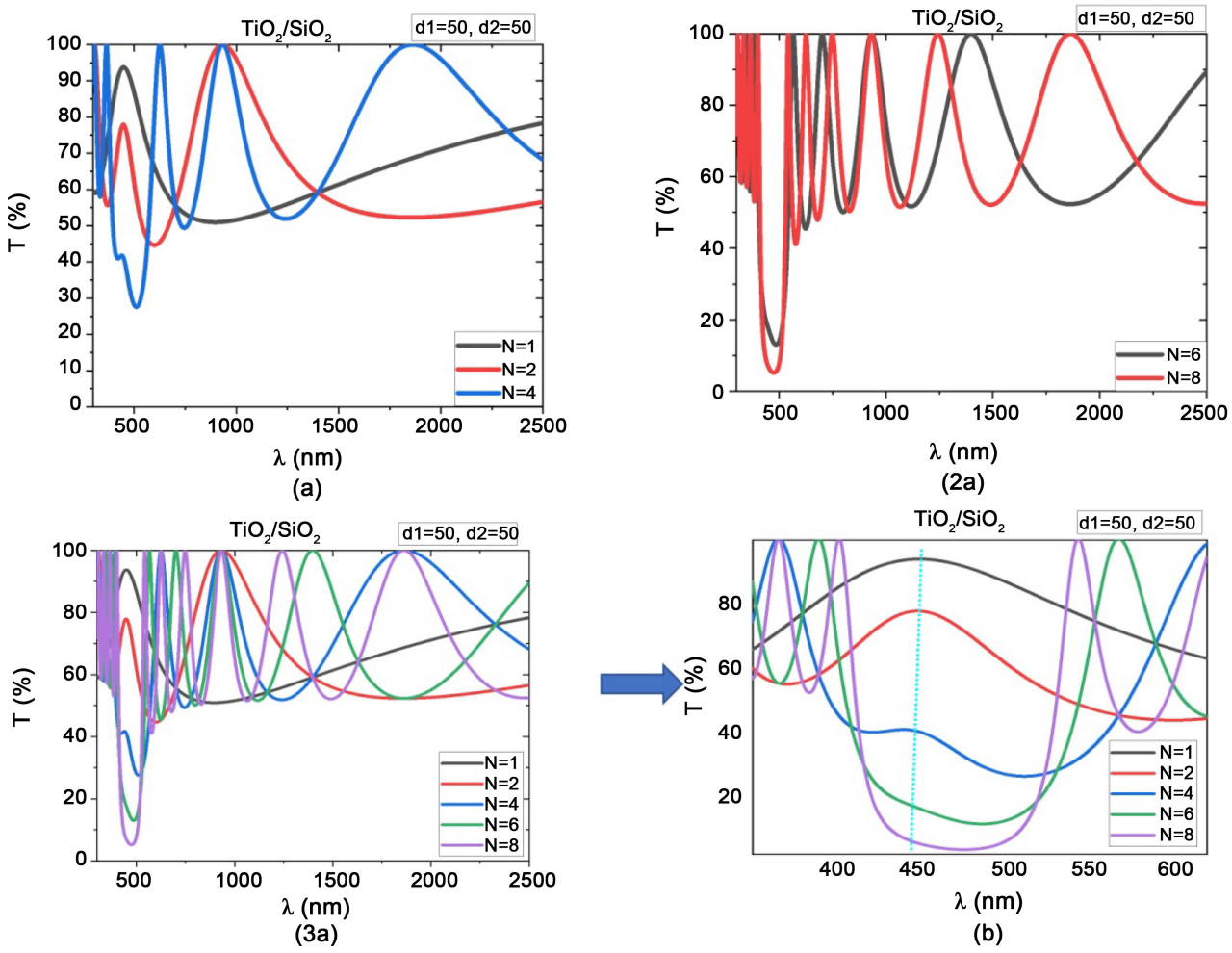

Figure 3. (a) The whole transmission spectrum for TiO_2/SnO_2 1D PhCs with varying numbers of layers (N = 1 to 8). (b) The bandgap region of (a) can be magnified to explain the widths and positions of each curve at varying layer numbers.

3) Comparative study between TiO_2/SiO_2 and TiO_2/SnO_2 1D PhCs

We see different behaviors when we compare the different 1D PhCs studied above with 1, 2, and 4 layers (**Figure 4**). We saw the bandgap appear first for TiO_2/SiO_2 at N = 2, and a clear shift to a lower wavelength is also observed. As the number of layers increase to 6 and 8, the width of the photonic bandgap becomes wider for TiO_2/SiO_2 when compared to TiO_2/SnO_2 (**Figure 5**). Moreover, at N = 8 the edges become even sharper and wider for TiO_2/SiO_2 when compared to TiO_2/SnO_2, and the photonic bandgaps were zero T and ~10% T, respectively. In general, this result agrees with the experimental and theoretical work of F. Javier Ramos *et al.* [39].

While we previously restricted our analysis to systems with a fixed layer thickness, different thicknesses should produce different properties. For example, we see a clear difference in the position and width of the bandgaps and transmission peaks when the thickness is changed from 50 nm/50 nm to 150 nm/150 nm or 300 nm/150 nm (**Figure 6**). Specifically, TiO_2/SiO_2 has a wider photonic bandgap from 350 - 500 nm, whereas TiO_2/SnO_2 has a bandgap from

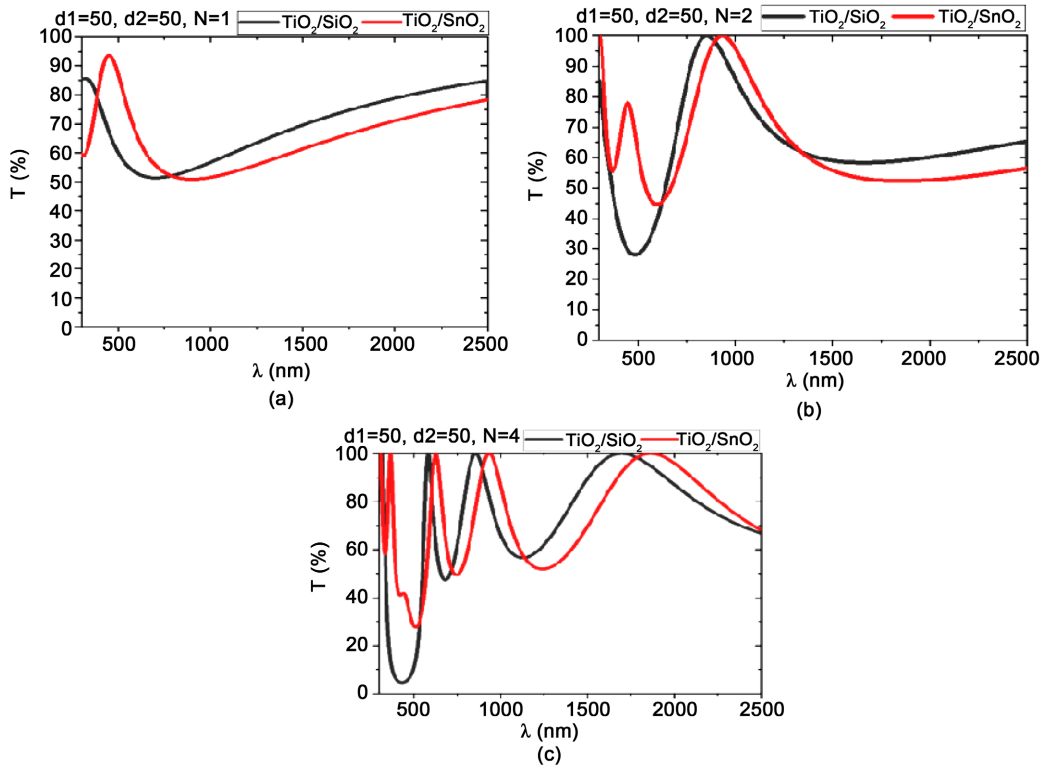

Figure 4. Comparative study of TiO_2/SiO_2 and TiO_2/SnO_2 at different layer numbers (N= 1 (a), 2 (b), and 4 (c)) with a layer thickens of 100 nm (50 nm/50nm).

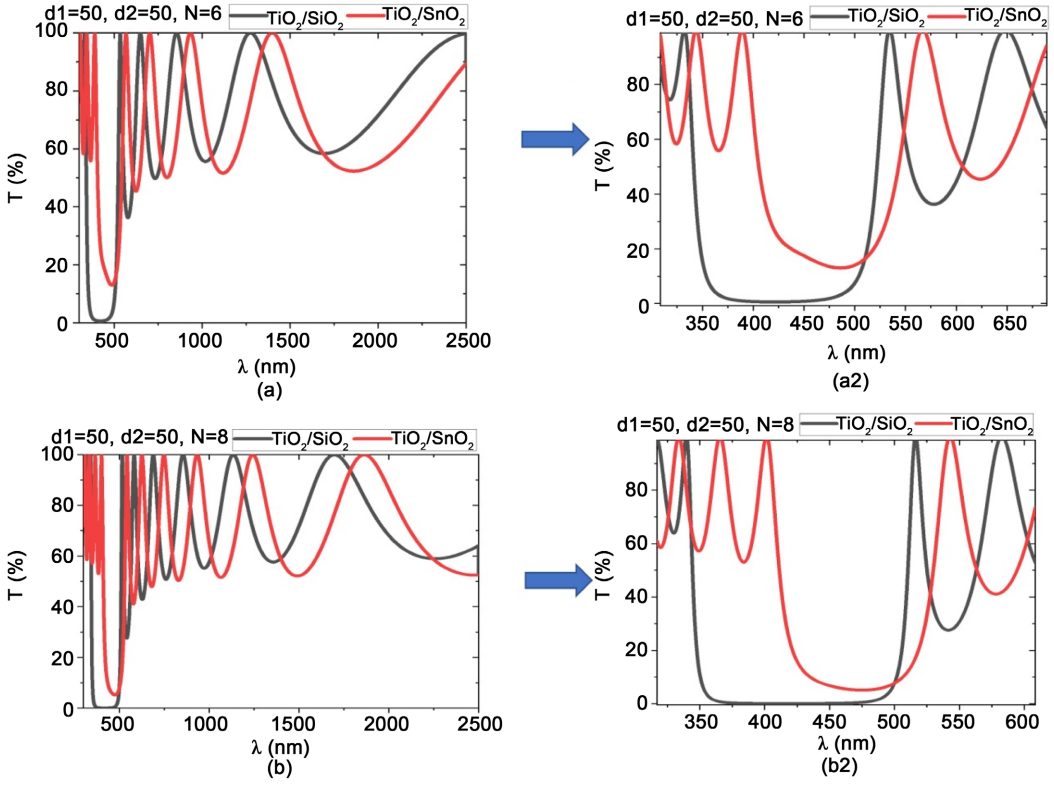

Figure 5. Comparative study of TiO_2/SiO_2 and TiO_2/SnO_2 at different layer numbers (N= 6 (a) and 8 (b)) with a layer thickedns of 100 nm (50 nm/50 nm).

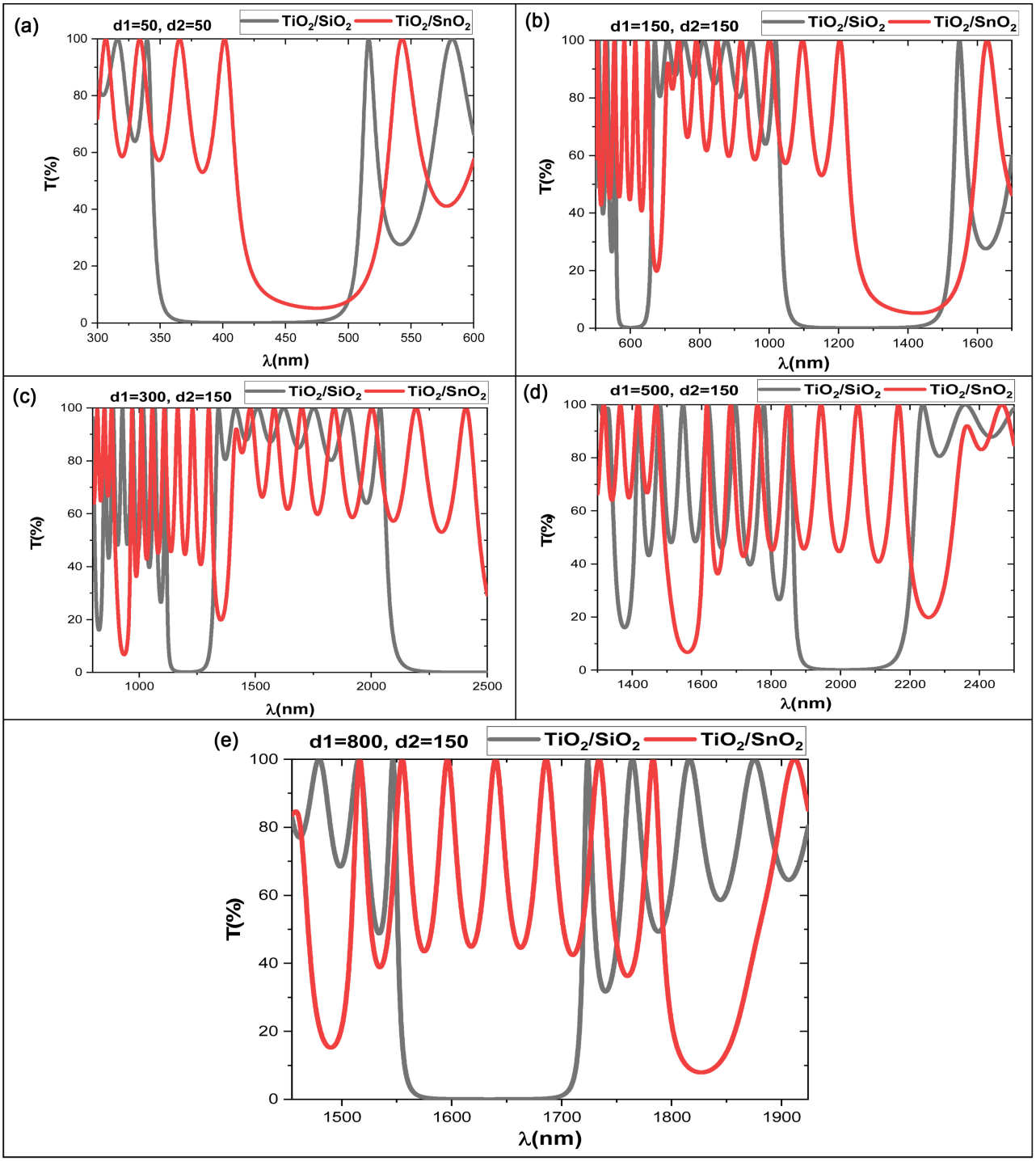

Figure 6. Thickness effects of 50 nm/50 nm, 150 nm/150 nm, and 300 nm/150 nm for TiO_2/SiO_2 and TiO_2/SnO_2 films. Thickness effects of 500 nm/150 nm (d) and 800 nm/150nm (e).

450 - 550 nm without sharp edges that shifted slightly to longer wavelengths under the same conditions. Moreover, we could better observe two photonic bandgaps for TiO_2/SiO_2 when the thickness was increased to 150 nm/150 nm, where higher thicknesses had an even more pronounced effect on the transmission behavior. The TiO_2/SiO_2 films exhibited high transmittance and a wide

bandgap for systems with thicknesses of 500 nm/150nm and 800 nm/150nm (Figure 6), which supports a wide range of optical filter applications. However, in the case of TiO_2/SnO_2, these thicker structures could support a single optical detector. The dependence on layer number and thickness motivated us to investigate SiO_2/SnO_2.

4) 1D SiO_2/SnO_2 PhCs

SiO_2/SnO_2 materials have previously been studied in a variety of applications such as sensors, thin films, and transparent ceramic electrodes due to their transparency in the visible and near-infrared parts of the electromagnetic spectrum. Several studies have been carried out in order to realize and demonstrate the photorefractive effect of SiO_2/SnO_2 glass-ceramics for photonic applications, as well as the role of SnO_2 nanocrystals as rare-earth luminescence sensitizers [40]. Specifically, UV irradiation causes a change in the refractive index, which allows for the direct writing of channel waveguides and Bragg gratings. We continued our comparison study of SiO_2/SnO_2 using TMM and the same structural parameters used above. By increasing the number of layers, we did not see a clear photonic bandgap at $N = 1$ or 2. The lowest T was observed at $N = 8$, while the highest T occurred at $N = 4$. Specifically, increasing the layer number enhances the homogeneity of the films due to the high interference probability (Figure 7). It is interesting to note that there is some consistency in the optical

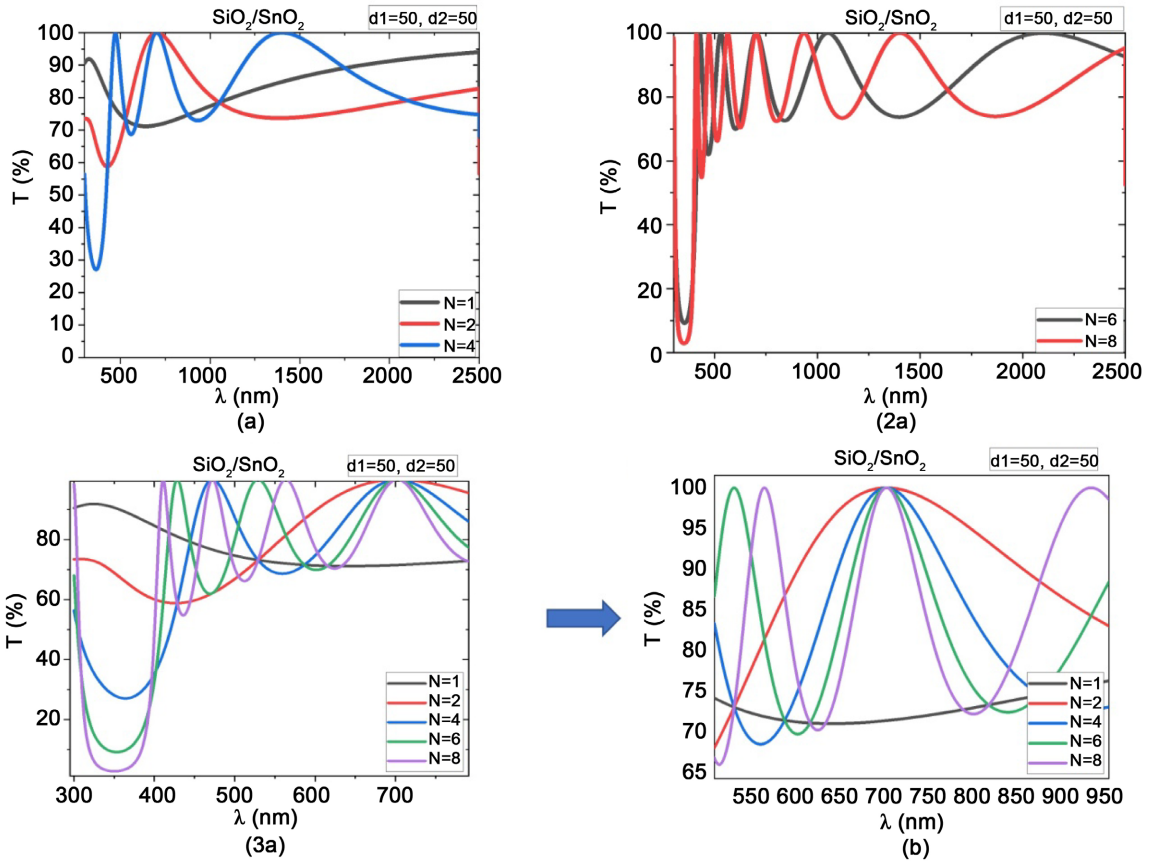

Figure 7. The effect of layer number on the transmittance of 1D SiO_2/SnO_2 PhCs.

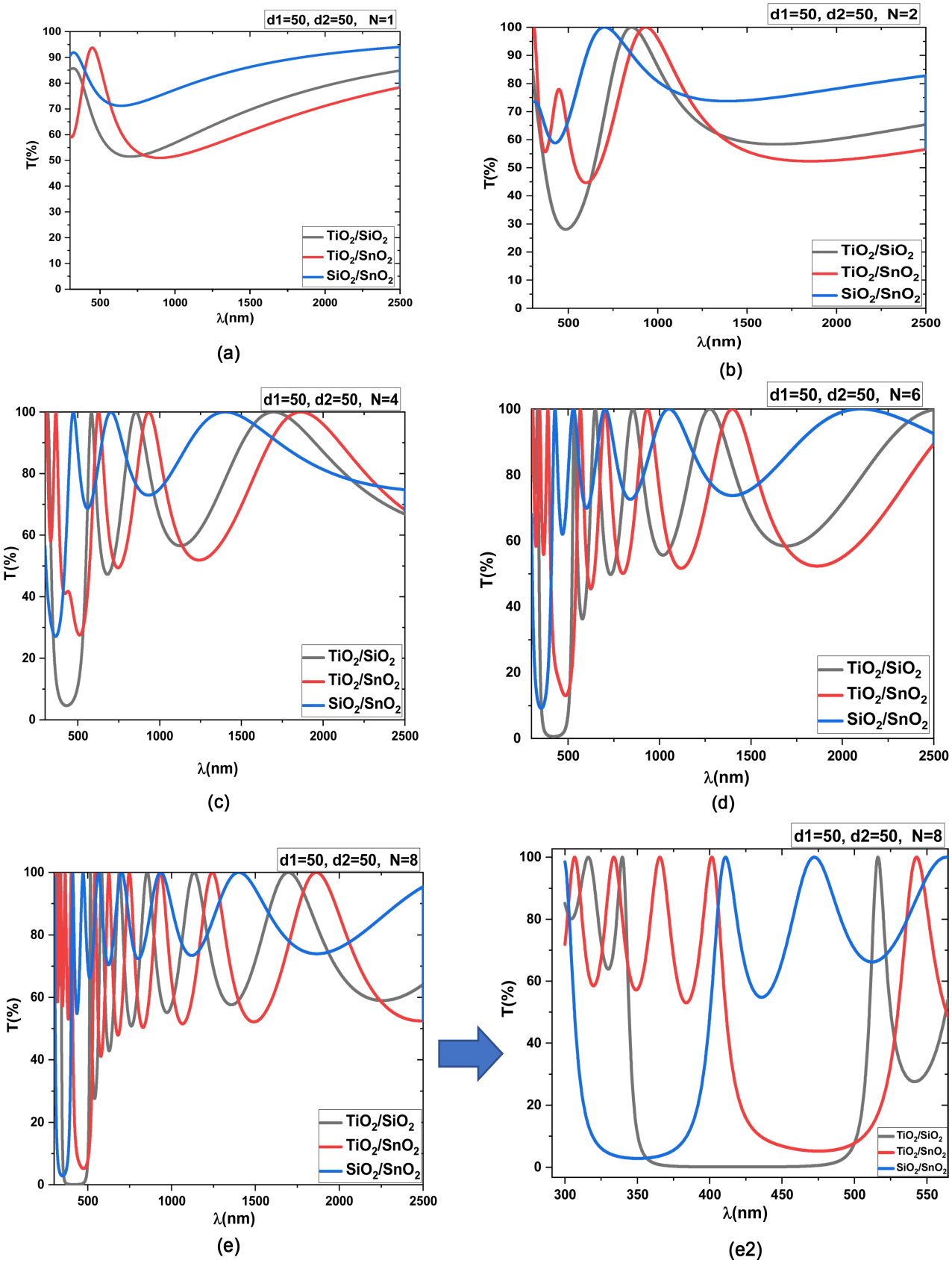

Figure 8. Effect of layer number (N= 1 (a), 2 (b), 4 (c), and 6 (d)), on transmittance for different 1D PhCs.

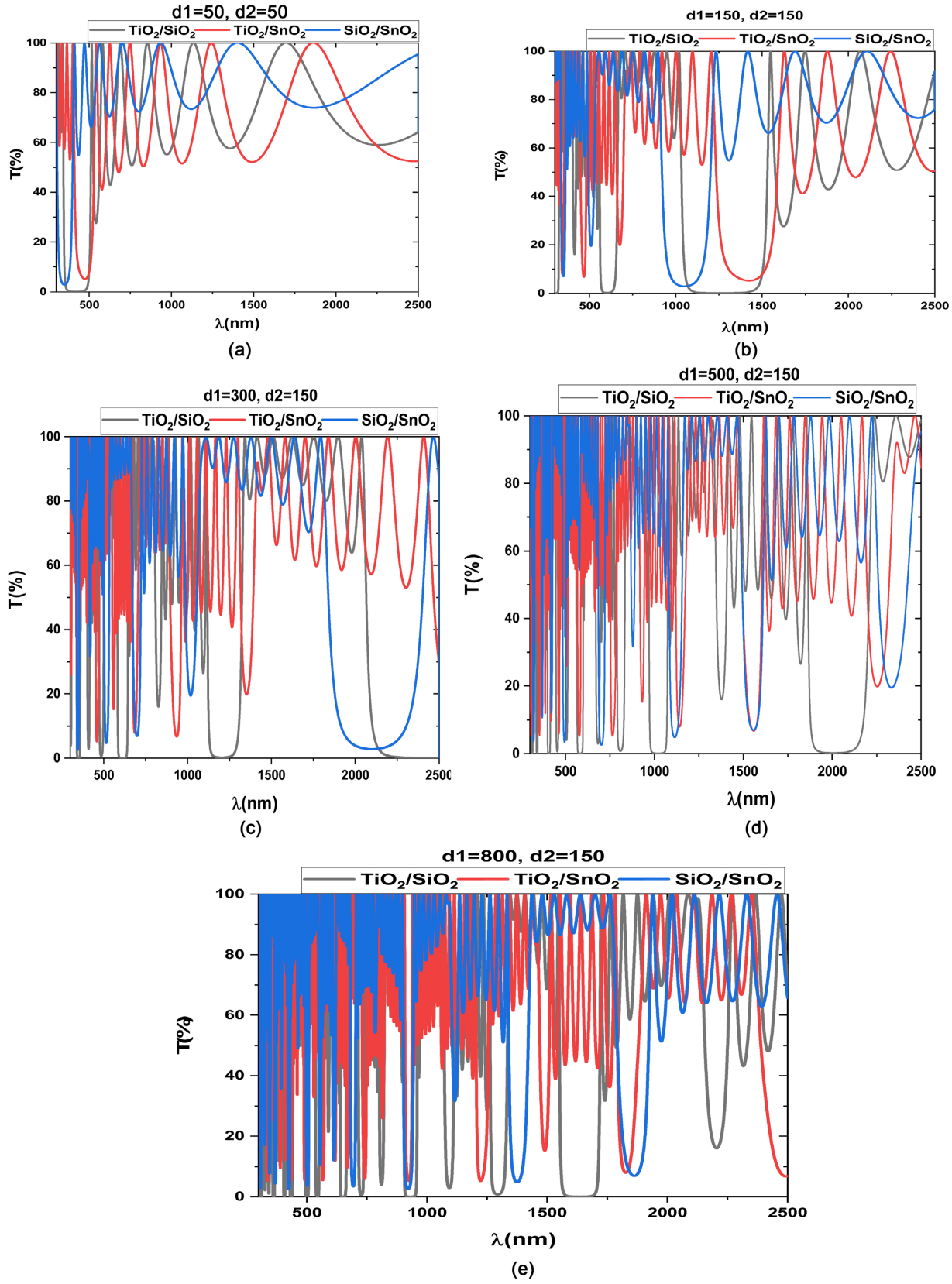

Figure 9. Comparison of the effects of thickness when changing from 50 nm/50nm (a), 150 nm/150nm (b), to 300 nm/150nm (c) at 500 nm/150nm (d), and 800 nm/150nm (e) for all three 1D PhC systems.

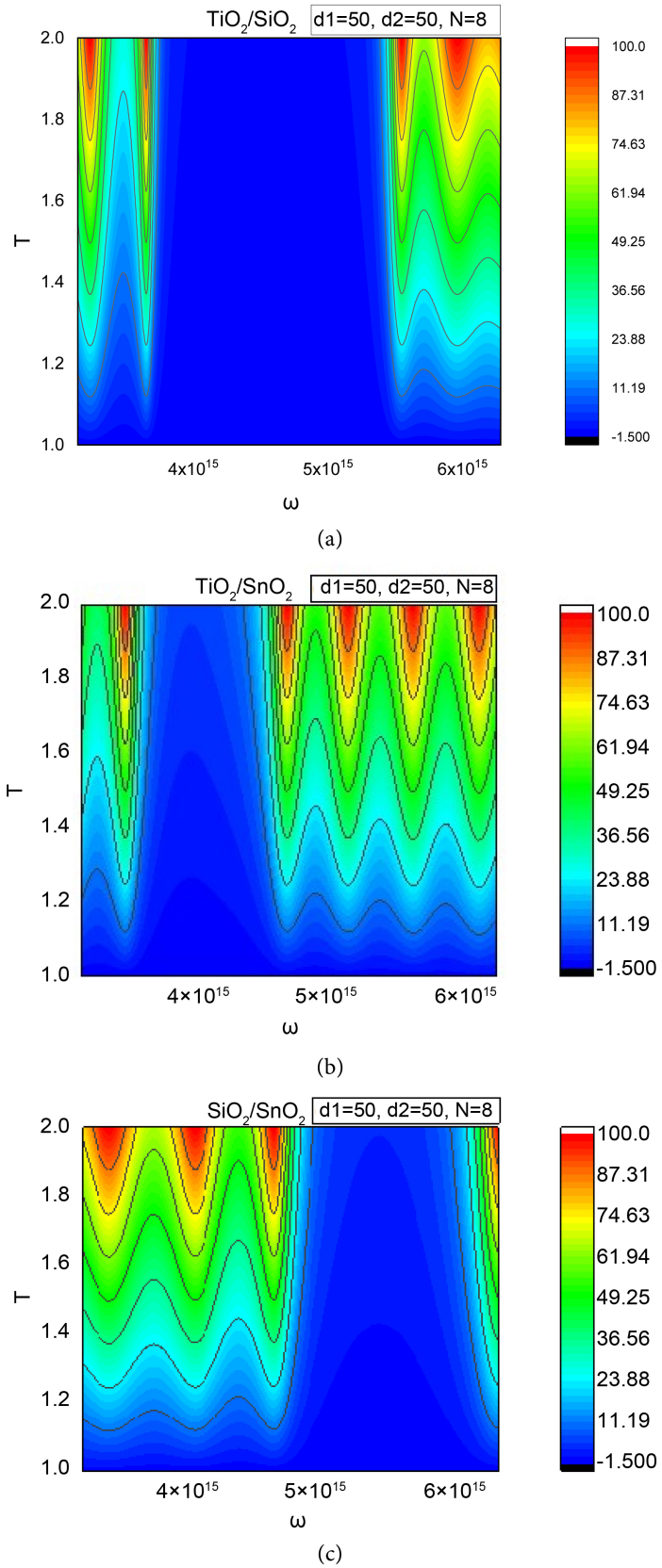

Figure 10. Transmissivity, T, as a function of the angular frequency for three structures at $N = 8$.

waves around $\lambda = 700$ nm.

5) Comparative study of the three different 1D PhCs

The SiO_2/SnO_2 PhC almost had a higher T than the TiO_2-based PhCs, particularly in the visible region. Specifically, the SiO_2/SnO_2 peak was at lower wavelengths, *i.e.*, the UV region, compared to the TiO_2 systems. Interestingly, the bandgap for TiO_2/SiO_2 appears at $N = 2$, but for the other two systems does not appear until $N = 4$. The SiO_2/SnO_2 transmission curve was more concentrated in the UV region when compared to the other curves. The TiO_2/SnO_2 curve had a higher wavelength shift, whereas the TiO_2/SiO_2 curve had the lowest T value (Figure 8). The smooth/single wavelength transition was present in all three curves for $N = 4$, confirming they are compatible with single wavelength devices and applications. When the number of layers is increased to $N = 6$, there was no change in the bandgap position, but there was a widening of the bandgap that was magnified further at $N = 8$. The photonic bandgap in SiO_2/SnO_2 was centered at 350 nm and extends through the UV region, while the TiO_2/SnO_2 bandgap was centered at 480 nm and the TiO_2/SiO_2 photonic bandgap at 430 nm, both in the visible region.

The effect of layer thickness on the transmittance of the different 1D PhCs was studied, however, the thickness of the bottom layer produced no discernible differences. Therefore, we decided to test varying the top thicknesses at $N = 8$ (Figure 9). At a layer thickness of 150 nm/150 nm, we can see that the bandgap shifted to the NIR region with two narrow bandgaps and one wide bandgap. When compared to the other two systems, SiO_2/SnO_2 had a higher transmittance. Generally, the photonic bandgap shifted to a longer wavelength at a layer thickness of 300 nm/150 nm. Surprisingly, the SiO_2/SnO_2 structure had only one photonic bandgap, while the other structures had multiple bandgaps. As a result, 1D SiO_2/SnO_2 PhCs could potentially be applied as one-photonic bandgap photonic devices. TiO_2/SiO_2 had a multi-channel photonic bandgap at all times and the T values were always greater than those of the other structures, making it particularly promising for multi-channel optical devices. Also, differences in angular frequency and transmission dependency for three structures were also reported in (Figure 10).

4. Conclusion

PhCs are arranged in periodic high-low dielectric patterns to control the penetration of light through structures, which opens the door to a wide range of nanotechnology and photovoltaic applications. Despite the fact that 3D PhCs are widely used in various applications, 1D PhCs are gaining popularity due to their fascinating optical properties and ease of fabrication. We conducted a theoretical analysis of 1D PhCs composed of TiO_2/SiO_2, TiO_2/SnO_2, and SiO_2/SnO_2. Specifically, we found that the bandgap appears first when using TiO_2/SiO_2, and there is a clear shift to lower wavelengths. By increasing the number of layers to $N = 6$ or 8, we see that the edges grow wider and sharper and the width of the photonic

bandgaps becomes wider for TiO_2/SiO_2 when compared to TiO_2/SnO_2. Moreover, in TiO_2/SiO_2, the photonic bandgap reaches zero T, whereas it does not reach this for TiO_2/SnO_2. Thick TiO_2/SiO_2 films exhibit high transmittance for wide bandgaps, which supports their use in a wide range of optical filter applications. On the other hand, TiO_2/SnO_2 can support a single wavelength optical detector. Interestingly, we did not see a clear photonic bandgap at $N = 1$ or 2 when combining SiO_2 and SnO_2, and at higher layer numbers only had one bandgap centered at 350 nm through the UV region, whereas the other systems have many. Specifically, TiO_2/SnO_2 shows a bandgap centered at 480 nm, while TiO_2/SiO_2 is centered at 430 nm. In terms of the effect of thickness, for large thicknesses, the TiO_2/SiO_2 film showed high transmittance for wide bandgaps, and the SiO_2/SnO_2 structure only had one photonic bandgap, whereas the others have many. TiO_2/SiO_2 always showed a multi-channel photonic bandgap.

Acknowledgements

Authors are thankful to Alfaisal University for providing MATLAB®.

Conflicts of Interest

The authors declare no conflicts of interest regarding the publication of this paper.

References

[1] Vlasov, Y.A., O'Boyle, M., Hamann, H.F. and McNab, S.J. (2005) Active Control of Slow Light on a Chip with Photonic Crystal Waveguides. *Nature*, **438**, 65-69. https://doi.org/10.1038/nature04210

[2] Liu, W., Ma, H. and Walsh, A. (2019) Advance in Photonic Crystal Solar Cells. *Renewable and Sustainable Energy Reviews*, **116**, Article ID: 109436. https://doi.org/10.1016/j.rser.2019.109436

[3] Söllner, I., Mahmoodian, S., Hansen, S.L., Midolo, L., Javadi, A., Kiršanskė, G., Pregnolato, T., El-Ella, H., Lee, E.H., Song, J.D., Stobbe, S. and Lodahl, P. (2015) Deterministic Photon-Emitter Coupling in Chiral Photonic Circuits. *Nature Nanotechnology*, **10**, 775-778. https://doi.org/10.1038/nnano.2015.159

[4] Barik, S. and Karasahin, A. (2018) A Topological Quantum Optics Interface. *Science*, **359**, 666-668. https://doi.org/10.1126/science.aaq0327

[5] Noda, S., Chutinan, A. and Imada, M. (2000) Trapping and Emission of Photons by a Single Defect in a Photonic Bandgap Structure. *Nature*, **407**, 608-610. https://doi.org/10.1038/35036532

[6] Deng, K. and Li, L. (2020) Optical Design in Perovskite Solar Cells. *Small Methods*, **4**, Article ID: 1900150. https://doi.org/10.1002/smtd.201900150

[7] Benisty, H., Chelnokov, A., Combrié, S. and Checoury, X. (2006) Recent Advances toward Optical Devices in Semiconductor-Based Photonic Crystals. *Proceedings of the IEEE*, **94**, 997-1023. https://doi.org/10.1109/JPROC.2006.873441

[8] Almeida, R. and Portal, S. (2003) Photonic Band Gap Structures by Sol-Gel Processing. *Current Opinion in Solid State and Materials Science*, **7**, 151-157. https://doi.org/10.1016/S1359-0286(03)00045-7

[9] Betancur, R., Romero-Gomez, P., Martinez-Otero, A., Elias, X., Maymó, M. and Martorell, J. (2013) Transparent Polymer Solar Cells Employing a Layered Light-Trapping Architecture. *Nature Photonics*, **7**, 995-1000. https://doi.org/10.1038/nphoton.2013.276

[10] Bermel, P., Luo, C., Zeng, L., Kimerling, L.C. and Joannopoulos, J.D. (2007) Improving Thin-Film Crystalline Silicon Solar Cell Efficiencies with Photonic Crystals. *Optics Express*, **15**, 16986-17000. https://doi.org/10.1364/OE.15.016986

[11] Zaky, Z.A. and Aly, A.H. (2020) Theoretical Study of a Tunable Low-Temperature Photonic Crystal Sensor Using Dielectric-Superconductor Nanocomposite Layers. *Journal of Superconductivity and Novel Magnetism*, **33**, 2983-2990. https://doi.org/10.1007/s10948-020-05584-1

[12] Mamri, B. and Barkat, O. (2019) Design of a Selective Filter Based on One-Dimensional Superconductor Photonic Crystal. *Journal of Superconductivity and Novel Magnetism*, **32**, 3397-3405. https://doi.org/10.1007/s10948-019-5118-0

[13] Deng, K. and Li, L. (2020) Optical Design in Perovskite Solar Cells. *Small Methods*, **4**, Article ID: 1900150. https://doi.org/10.1002/smtd.201900150

[14] Wu, H. and Kuang, Y. (2022) Propagation Characteristics of Flexural Wave in One-Dimensional Phononic Crystals Based on Lattice Dynamics Model. *Journal of Applied Mathematics and Physics*, **10**, 1416-1431. https://doi.org/10.4236/jamp.2022.105100

[15] Hui, R. (2019) Introduction to Fiber-Optic Communications. Elsevier, Amsterdam. https://doi.org/10.1016/B978-0-12-805345-4.00001-9

[16] Lourtioz, J.M., Benisty, H., Berger, V., Gérard, J.-M., Maystre, D. and Tchelnokov, A. (2006) Photonic Crystals: Towards Nanoscale Photonic Devices. *Physics Today*, **59**, Article No. 54. https://doi.org/10.1063/1.2349736

[17] Robinson, S. and Nakkeeran, R. (2013) Photonic Crystal Ring Resonator Based Optical Filters. IntechOpen, London. https://doi.org/10.5772/54533

[18] Singh, S.P. and Dipanjan, D. (2017) Dense and Narrow Stop-Bands Structure Based on One Dimensional Photonic Crystal Filter for Optical Communication. *International Journal of Engineering Science and Computing*, **7**, 15312-15316.

[19] Omid, B., Abdolrahim, B. and Ali, B. (2019) Disorder Effect on the Transmission of Second Harmonic Waves in One-Dimensional Periodically Poled $LiTaO_3$. *Journal of Modern Physics*, **10**, 432-442. https://doi.org/10.4236/jmp.2019.104028

[20] Tanaka, H., Takai, I., Fujikawa, H. and Iizuka, H. (2018) Nearly Polarization-Independent Angular Filters Consisting of One-Dimensional Photonic Crystals Realized in the Visible Region. *Journal of Lightwave Technology*, **36**, 2517-2523. https://doi.org/10.1109/JLT.2018.2819943

[21] Liu, L., Dong, P., Liu, R., Zhou, Q., Wang, X., Yi, G. and Cheng, B. (2005) Preparation and Self-Assembly of Uniform TiO_2/SiO_2 Composite Submicrospheres. *Journal of Colloid and Interface Science*, **288**, 1-5. https://doi.org/10.1016/j.jcis.2004.11.048

[22] Choi, D.H., Nam, S., Jung, K. and Moon, J.H. (2018) 2D Photonic Crystal Nanodisk Array as Electron Transport Layer for Highly Efficient Perovskite Solar Cells. *Nano Energy*, **56**, 365-372. https://doi.org/10.1016/j.nanoen.2018.11.050

[23] Murthy, S., Effiong, P. and Fei, C.C. (2020) Metal Oxide Nanoparticles in Biomedical Applications. In: Al-Douri, Y., Ed., *Metal Oxide Powder Technologies*, Elsevier, Amsterdam, 233-251. https://doi.org/10.1016/B978-0-12-817505-7.00011-7

[24] Katsidis, C.C. and Siapkas, D.I. (2002) General Transfer-Matrix Method for Optical Multilayer Systems with Coherent, Partially Coherent, and Incoherent Interference.

Applied Optics, **41**, 3978-3987. https://doi.org/10.1364/AO.41.003978

[25] Markoš, P. and Soukoulis, C.M. (2008) Wave Propagation: From Electrons to Photonic Crystals and Left-Handed Materials. Princeton University Press, Princeton. https://doi.org/10.1515/9781400835676

[26] Pérez, E.X. (2007) Design, Fabrication and Characterization of Porous Silicon Multilayer Optical Devices. Universitat Rovira i Virgili, Tarragona.

[27] John, S. (1987) Strong Localization of Photons in Certain Disordered Dielectric Superlattices. *Physical Review Letters*, **58**, 2486-2489. https://doi.org/10.1103/PhysRevLett.58.2486

[28] Baba, T. (2008) Slow Light in Photonic Crystals. *Nature Photonics*, **2**, 465-473. https://doi.org/10.1038/nphoton.2008.146

[29] Sankir, N.D. and Sankir, M. (2017) Printable Solar Cells. John Wiley & Sons, New York. https://doi.org/10.1002/9781119283720

[30] Kumar, A., Singh, P., Pal, K., Kumar, N. and Thapa, K.B. (2020) Broadband Reflector of 1D Photonic Crystal Containing TiO_2/SiO_2 Material at Visible Region. *AIP Conference Proceedings*, **2220**, Article ID: 020068. https://doi.org/10.1063/5.0002138

[31] Saravanan, S. and Dubey, R.S. (2021) Ultraviolet and Visible Reflective TiO_2/SiO_2 Thin Films on Silicon Using Sol-Gel Spin Coater. *Nanosystems*: *Physics*, *Chemistry*, *Mathematics*, **12**, 311-316. https://doi.org/10.17586/2220-8054-2021-12-3-311-316

[32] Sedrati, H., Benachour, M., Dehdouh, H. and Bensaha, R. (2020) Tuning of the Stop-Band Position in the Visible Range of SiO_2/TiO_2 Bragg Reflectors by Doping TiO_2 with Transition Metals. *Optik*, **208**, Article ID: 164098. https://doi.org/10.1016/j.ijleo.2019.164098

[33] Álvarez, S.E.H. and Segovia-Chaves, F. (2019) Transmittance Spectrum TM in a Photonic Crystal TiO_2/SiO_2. *Optik*, **186**, 369-373. https://doi.org/10.1016/j.ijleo.2019.04.054

[34] Dalmis, R., Azem, N.F.A., Birlik, I. and Celik, E. (2019) SiO_2/TiO_2 One-Dimensional Photonic Crystals Doped with Sm and Ce Rare-Earth Elements for Enhanced Structural Colors. *Applied Surface Science*, **475**, 94-101. https://doi.org/10.1016/j.apsusc.2018.12.234

[35] Hinczewski, D., Hinczewski, M., Tepehan, F. and Tepehan, G. (2005) Optical Filters from SiO_2 and TiO_2 Multi-Layers Using Sol-Gel Spin Coating Method. *Solar Energy Materials and Solar Cells*, **87**, 181-196. https://doi.org/10.1016/j.solmat.2004.07.022

[36] Das, S. and Jayaraman, V. (2014) SnO_2: A Comprehensive Review on Structures and Gas Sensors. *Progress in Materials Science*, **66**, 112-255. https://doi.org/10.1016/j.pmatsci.2014.06.003

[37] Lopez-Torres, D., Elosua, C., Villatoro, J., Zubia, J., Rothhardt, M., Schuster, K. and Arregui, F.J. (2017) Enhancing Sensitivity of Photonic Crystal Fiber Interferometric Humidity Sensor by the Thickness of SnO_2 Thin Films. *Sensors and Actuators B*: *Chemical*, **251**, 1059-1067. https://doi.org/10.1016/j.snb.2017.05.125

[38] Chen, S.L., Wang, A.J., Dai, C., Benziger, J.B. and Liu, X.C. (2014) The Effect of Photonic Band Gap on the Photo-Catalytic Activity of nc-TiO_2/SnO_2 Photonic Crystal Composite Membranes. *Chemical Engineering Journal*, **249**, 48-53. https://doi.org/10.1016/j.cej.2014.03.075

[39] Ramos, F.J., Oliva-Ramírez, M., Nazeeruddin, M.K., Graetzel, M., Gonzalez-Elipe, A.R. and Ahmad, S. (2016) Light Management: Porous 1-Dimensional Nanocolumnar Structures as Effective Photonic Crystals for Perovskite Solar Cells. *Journal*

of Materials Chemistry A, **4**, 4962-4970. https://doi.org/10.1039/C5TA08743K

[40] Tran, T.N.L. (2019) Tin Dioxide-Based Photonic Glass-Ceramics. Ph.D. Dissertation, University of Trento, Trento.

Symbols and Abbreviations

θ_m: Angle of incidence for each layer.
ω: Angular frequency.
λ: Wavelength.
A: Absorptance.
c: The speed of light in a vacuum.
d: Thickness.
D_0: Air dynamical matrix.
D_m: Dynamical matrices.
K: Bloch wave number constant.
l: Layers of refractive index.
P_m: Propagation matrix.
PBG: Photonic band gap.
n_0: Refractive index at the interface.
n_m: Refractive index of the "m" layer.
n_s: Refractive index at the substrate.
N: Number of periods.
r: Reflection amplitude.
R: Reflectance.
SiO_2/SnO_2: Silicon dioxide/Tin dioxide.
t: Transmission coefficient.
T: Transmissivity.
TiO_2/SiO_2: Titanium dioxide/Silicon dioxide.
TiO_2/SnO_2: Titanium dioxide/Tin dioxide.
TMM: Transfer matrix method.
TE: Transverse Electric.